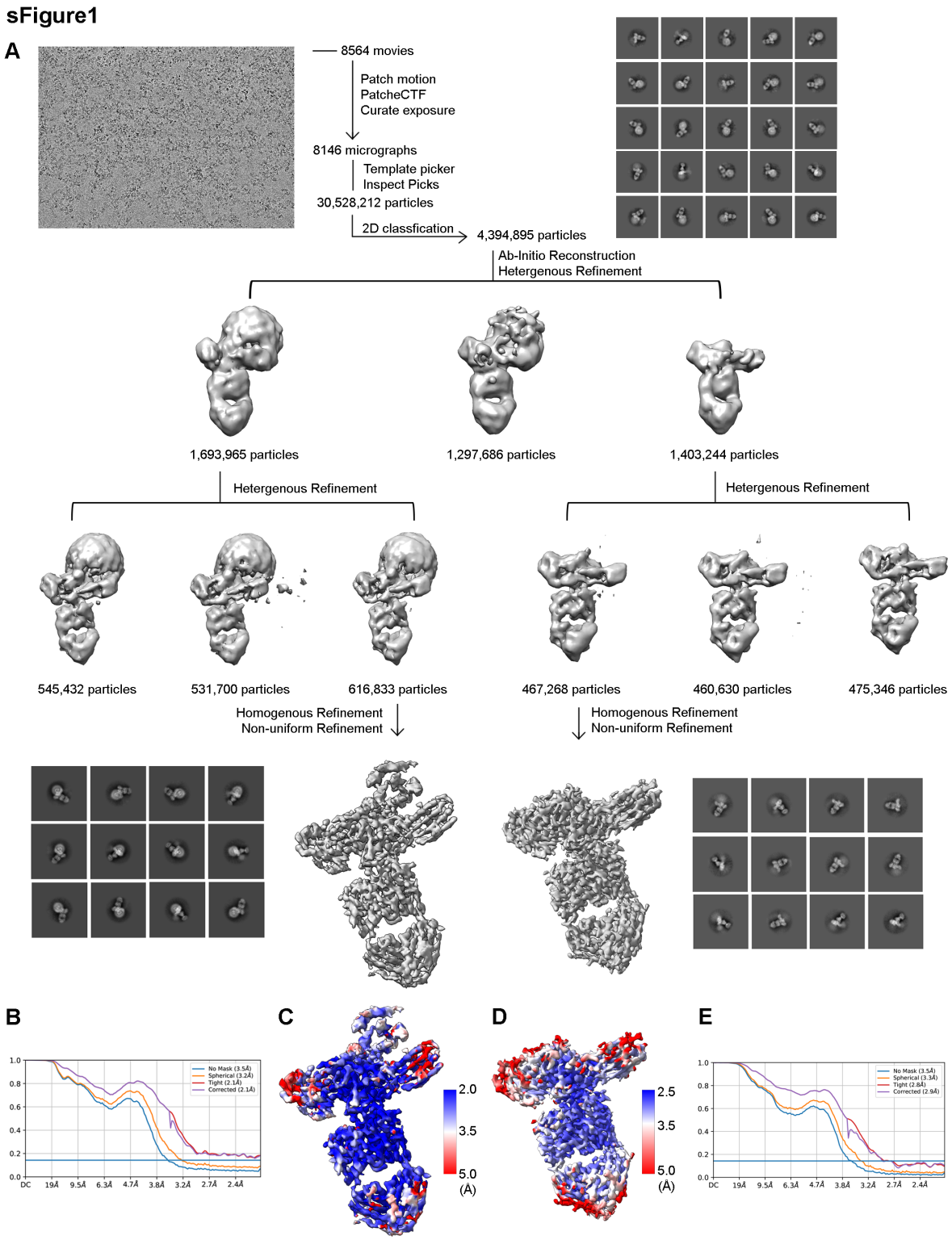


**Figure S1. Workflow of cryo-EM data processing and resolution analysis of pACKR3(GRK5)–Arr2–Fab7.** (A) Representative micrograph shows well-distributed complexes. The cryo-EM workflow from motion correction to CTF estimation to particle picking to 2D classification to 3D refinement is shown. (B, E) Fourier shell correlation (FSC) curves calculated by cryoSPARC with 0.143 as a cutoff for pACKR3(GRK5)–Arr2–Fab7 with (B) or without (E) the ACKR3 TM core. (C, D) Local resolution estimation calculated by cryoSPARC for pACKR3(GRK5)–Arr2–Fab7 with (C) or without (D) the ACKR3 TM core.

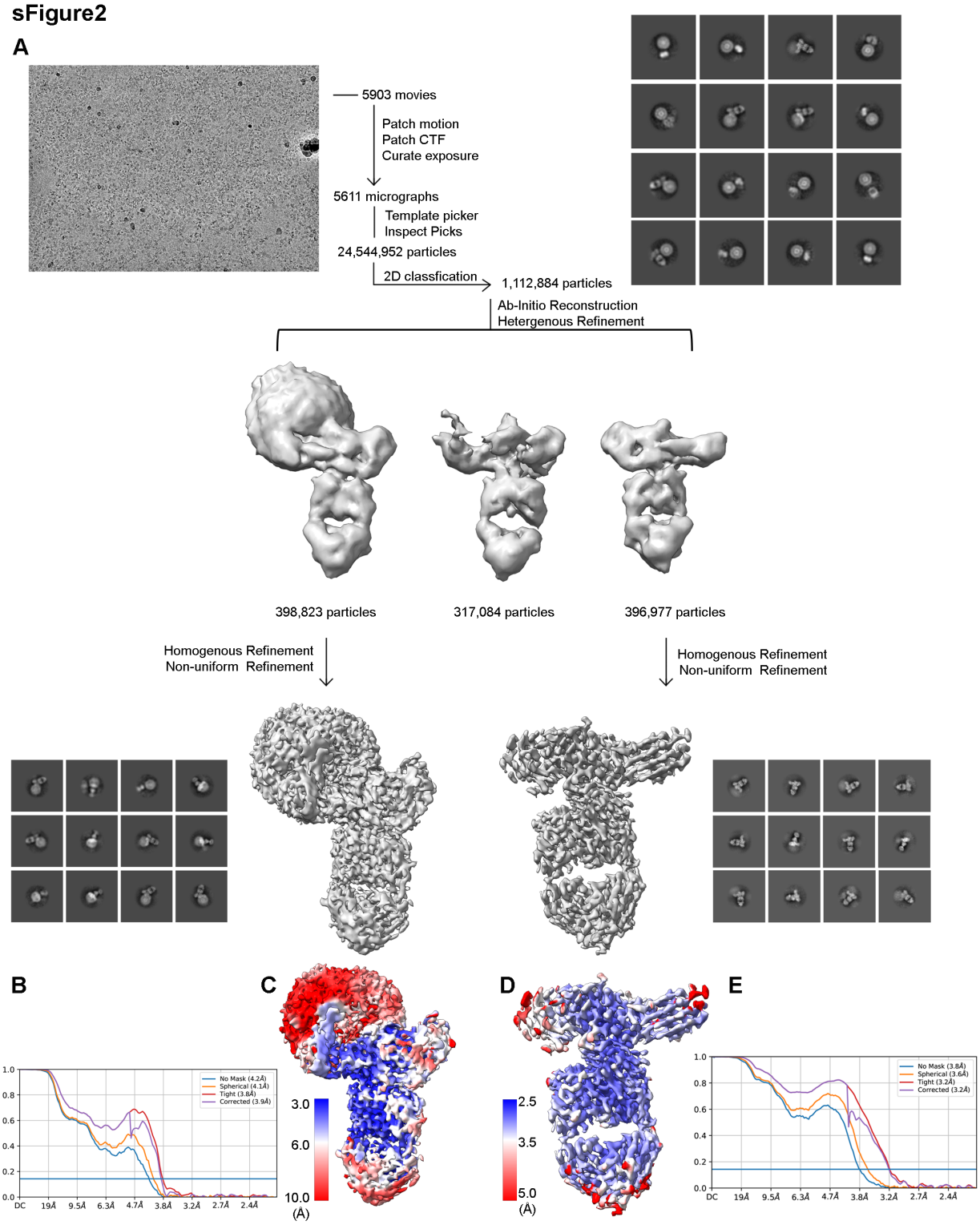


**Figure S2. Workflow of cryo-EM data processing and resolution analysis of pACKR3 (GRK2)–Arr2–Fab7.** (A) Representative micrograph shows well-distributed complexes. The cryo-EM data processing workflow from motion correction to CTF estimation to particle picking to 2D classification to 3D refinement is shown. (B, E) FSC curves calculated by cryoSPARC with 0.143 as a cutoff for pACKR3(GRK2)–Arr2–Fab7 with (B) or without (E) the ACKR3 TM core. (C, D) Local resolution estimation calculated by cryoSPARC for pACKR3(GRK2)–Arr2–Fab7 with (C) or without (D) the ACKR3 TM core.

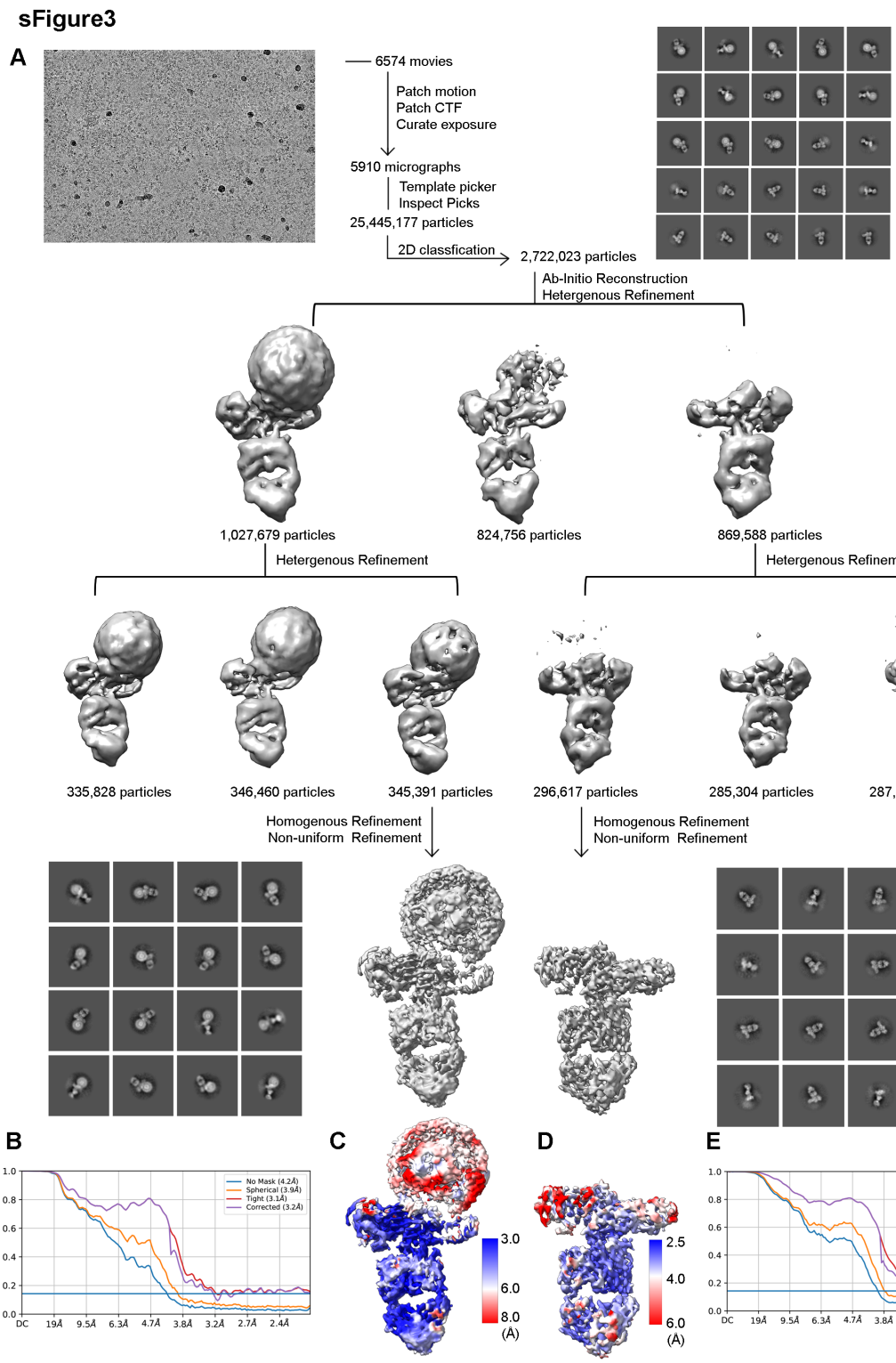


**Figure S3. Workflow of cryo-EM data processing and resolution analysis of pACKR3(GRK5)–Arr3–Fab7.** (A) Representative micrograph shows well-distributed complexes. The cryo-EM data processing workflow from motion correction to CTF estimation to particle picking to 2D classification to 3D refinement is shown. (B, E) FSC curves calculated by cryoSPARC with 0.143 as a cutoff for pACKR3(GRK5)–Arr3–Fab7 with (B) or without (E) the ACKR3 TM core. (C, D) Local resolution estimation calculated by cryoSPARC for pACKR3(GRK5)–Arr3–Fab7 with (C) or without (D) the ACKR3 TM core.

sFigure4

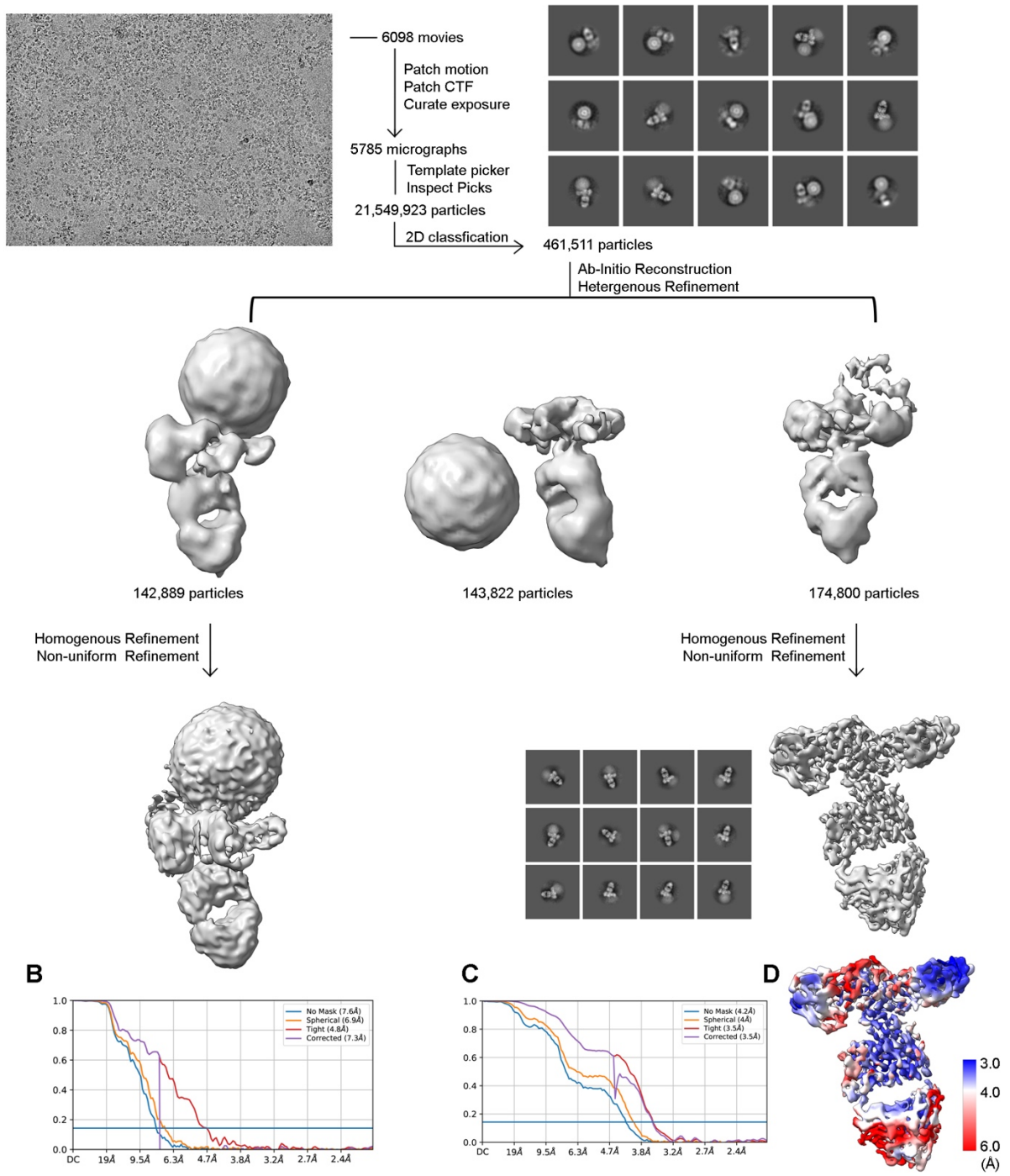


**Figure S4. Workflow of cryo-EM data processing and resolution analysis of pACKR3 (GRK2)–Arr3–Fab7.** (A) Representative micrograph shows well-distributed complexes. The cryo-EM data processing workflow from motion correction to CTF estimation to particle picking to 2D classification to 3D refinement is shown. (B, C) FSC curves calculated by cryoSPARC with 0.143 as a cutoff for pACKR3(GRK2)–Arr3–Fab7 with (B) or without (C) the ACKR3 TM core. (E) Local resolution estimation calculated by cryoSPARC for pACKR3(GRK2)–Arr2–Fab7 without the ACKR3 TM core.

**sFigure5**

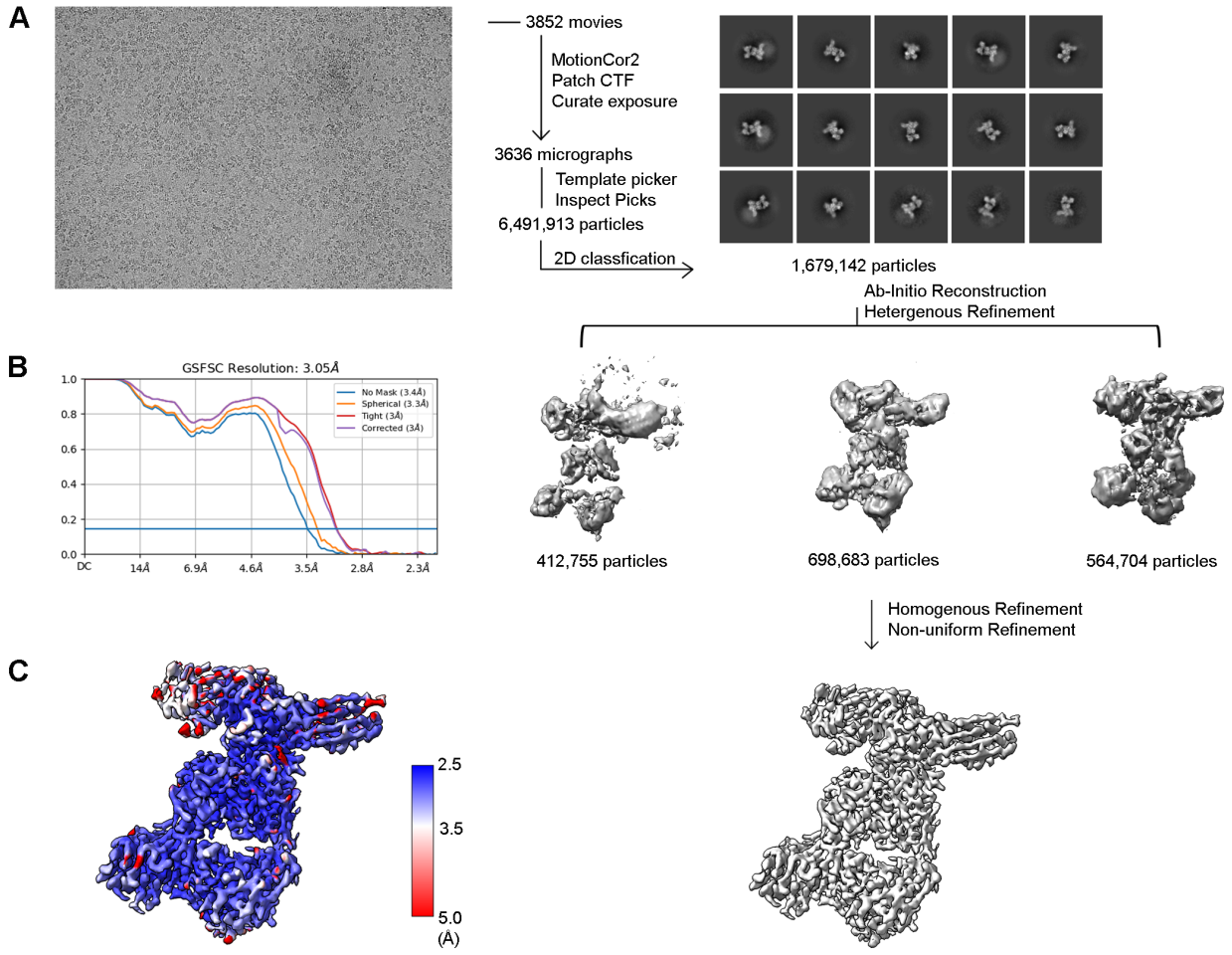


**Figure S5. Workflow of cryo-EM data processing and resolution analysis of pACKR3 (GRK2)–Arr2–Fab7 in nanodisc.** (A) Representative micrograph shows well-distributed complexes. The cryo-EM data processing workflow from motion correction to CTF estimation to particle picking to 2D classification to 3D refinement is shown. (B) FSC curves calculated by cryoSPARC with 0.143 as a cutoff for pACKR3(GRK2)–Arr2–Fab7 in nanodisc without the ACKR3 TM core. (E) Local resolution estimation calculated by cryoSPARC for pACKR3(GRK2)–Arr2–Fab7 without the ACKR3 TM core.

**sFigure6**

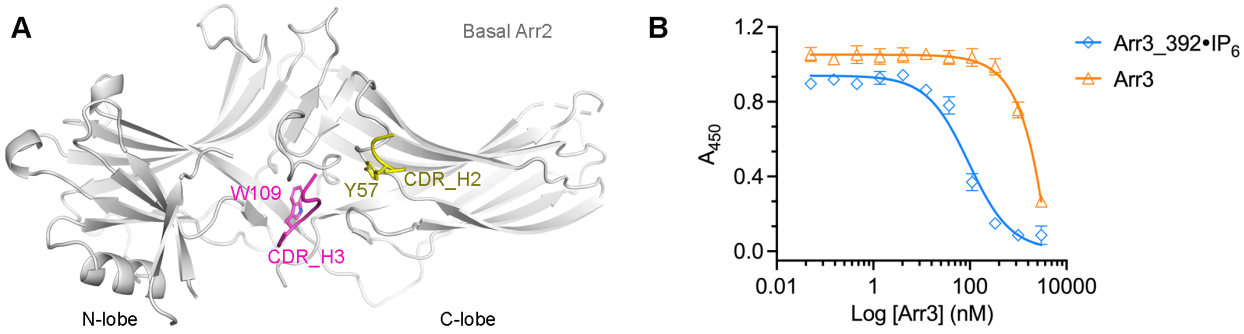


**Figure S6. Fab7 preferentially binds arrestin in its activated state.** (A) Superposition of basal Arr2 (light grey, PDB entry 1G4M) with activated Arr2 from the pACKR3(GRK2)–Arr2–Fab7 complex (only Fab7 shown, PDB entry XXXX) aligned on their Arr2 C-lobes. Some of the potential clashes expected to reduce affinity are highlighted. (B) ELISA analysis of Fab7 competition assay reveals that preactivated Arr3_392·$IP_6$ ($IC_{50}$ ~90 nM) competes for Fab7 binding more efficiently than WT Arr3 ($IC_{50}$ ~ 35 μM). Error bars represent S.D. from three technical replicates.

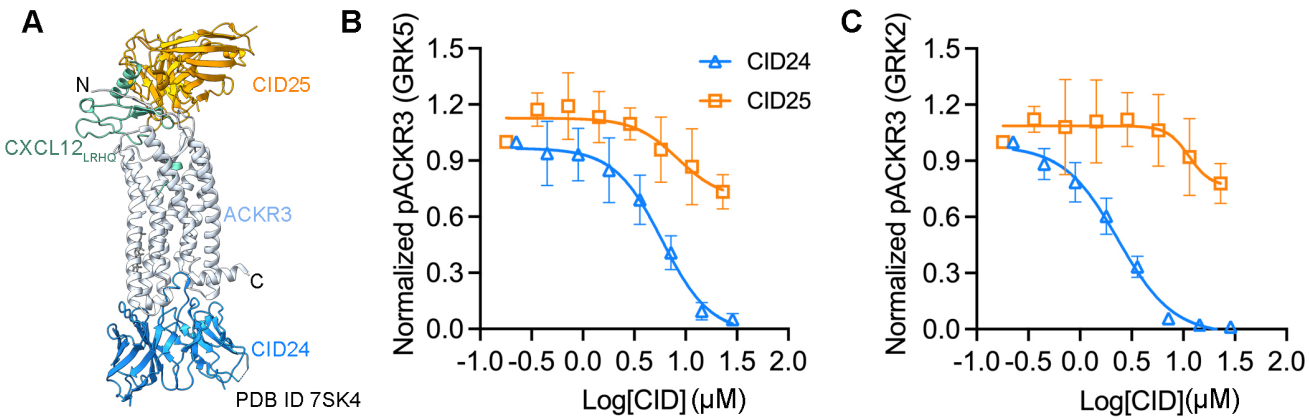


**Figure S7. CID24 efficiently blocks GRK2 and GRK5 phosphorylation of ACKR3.** (A) CID24 and CID25 bind to the intercellular and extracellular regions of ACKR3, respectively (PDB entry 7SK4). (B, C) ACKR3 phosphorylation by GRK5 (B) and GRK2 (C) in the presence of increasing amounts of CID24 or CID25.

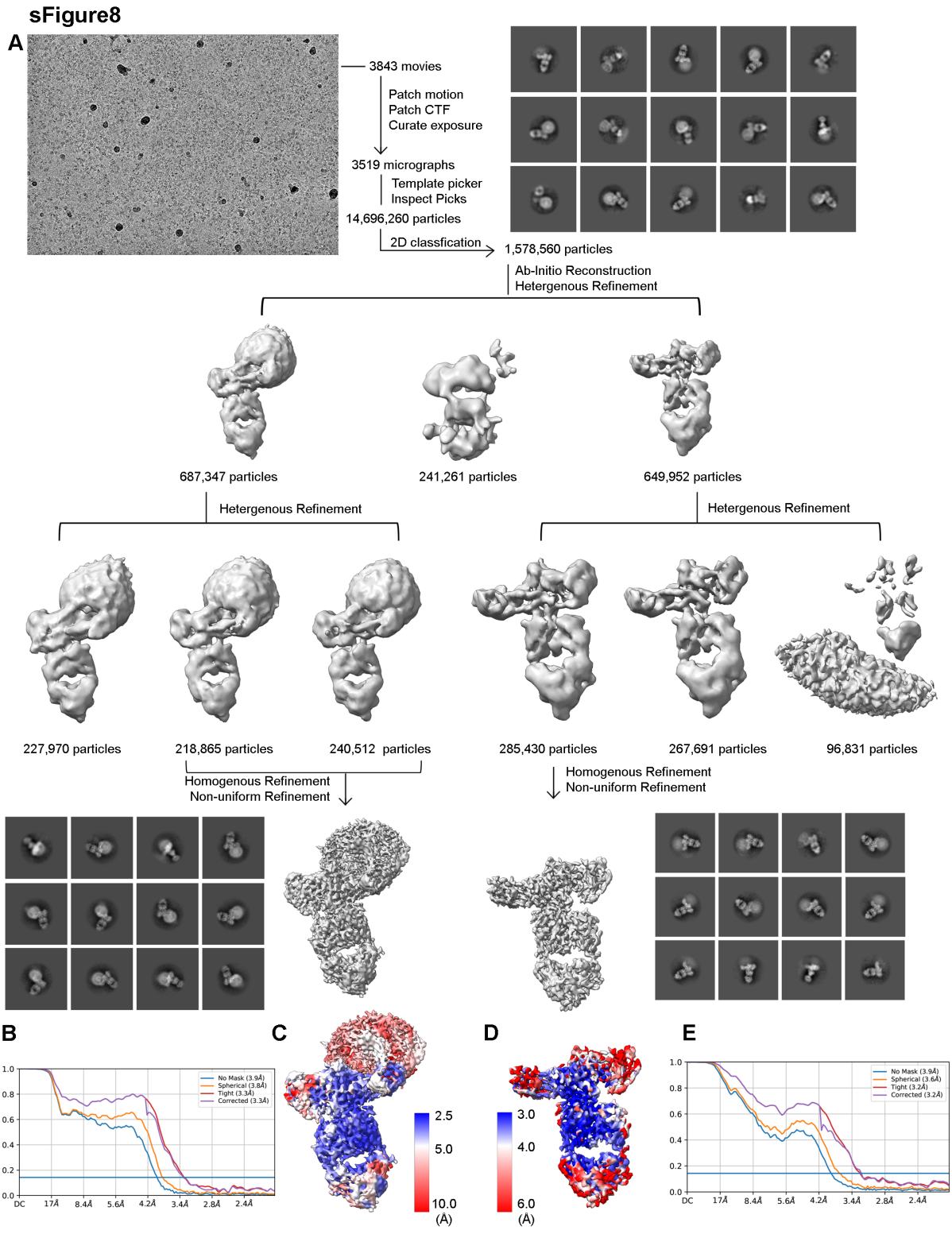


**Figure S8. Workflow of cryo-EM data processing and resolution analysis of pACKR3+12G(GRK5)–Arr2–Fab7.** (A) Representative micrograph shows well-distributed complexes. The cryo-EM data processing workflow from motion correction to CTF estimation to particle picking to 2D classification to 3D refinement is shown. (B, C) FSC curves calculated by cryoSPARC with 0.143 as a cutoff for pACKR3+12G(GRK5)–Arr2–Fab7 with (B) or without (C) the ACKR3 TM core. (E) Local resolution estimation calculated by cryoSPARC for pACKR3+12G(GRK5)–Arr2–Fab7 without the ACKR3 TM core.

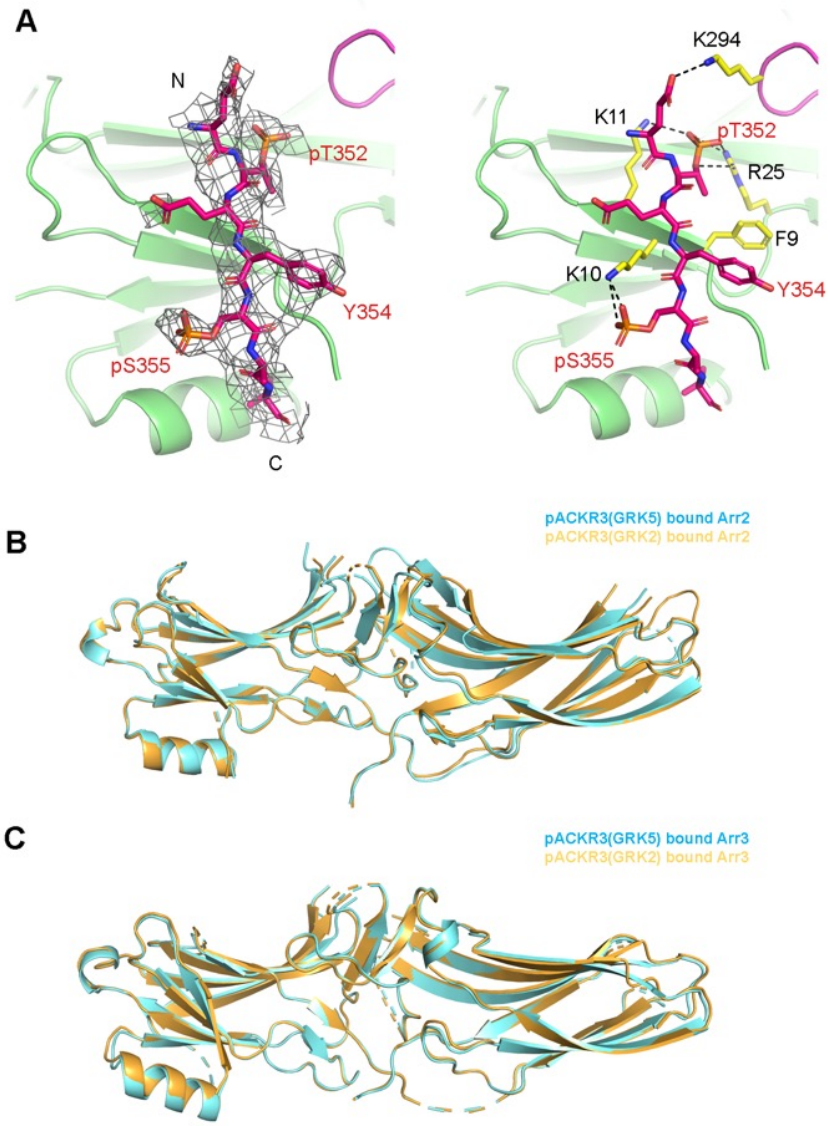


**Figure S9.** (A) Interactions of ACKR3 C-tail phosphorylated by GRK2 with Arr2 N-lobe in the pACKR3(GRK2)–Arr2–Fab7 complex in nanodisc. Electron density of ACKR3 GRK2 phospho-peptide is shown as a wire cage contoured at 4σ. Distances below 4 Å are shown as black dash line. (B, C) Alignment of pACKR3(GRK5) bound and pACKR3(GRK2) bound Arr2 (B) or Arr3 (C) on the N-lobe suggests subtle changes in arrestin conformation.

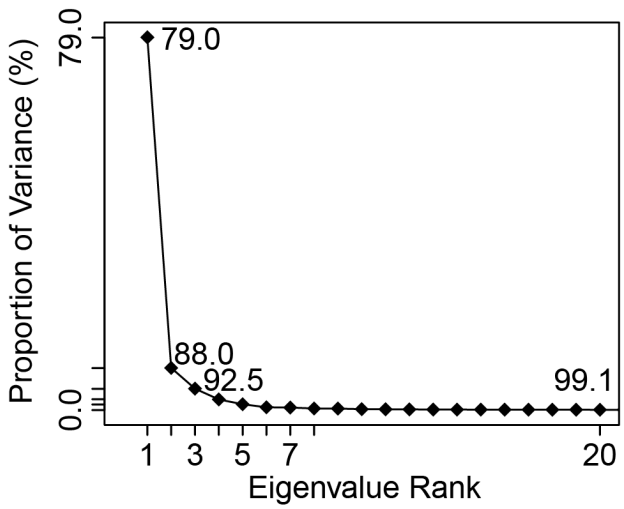


**Figure S10. Scree plot showing associated eigenvalues from PCA analysis of deposited arrestin structures (Figure 6A).** The eigenvalues measure the conformational variance along corresponding principal component axes, which usually decrease rapidly after the top few components, as occurs here.

**Table S1. Summary of determined cryo-EM maps and structures.**

| EMDB ID | PDB ID | ACKR3 | Arrestin | Phosphorylated by | Model membrane system | Resolution (Å) | Tail interaction? | Finger loop membrane insertion? | C-edge loop membrane insertion? |
|---|---|---|---|---|---|---|---|---|---|
| | | WT | Arr2_3A | GRK5 | LMNG | 3.2 | Y | Y | Y |
| | | WT | Arr2_3A | GRK2 | LMNG | 4.1 | Y | Y | Y |
| | | WT | Arr3_ΔC | GRK5 | LMNG | 3.9 | Y | Y | N |
| | | WT | Arr3_ΔC | GRK2 | LMNG | 6.9 | Y | Y | N |
| | | +12G | Arr2_3A | GRK5 | LMNG | 3.8 | Y | Y | Y |
| | | WT | Arr2_3A | GRK5 | LMNG | 3.3 | Y | N/A | N/A |
| | | WT | Arr2_3A | GRK2 | LMNG | 3.6 | Y | N/A | N/A |
| | | WT | Arr3_ΔC | GRK5 | LMNG | 3.8 | Y | N/A | N/A |
| | | WT | Arr3_ΔC | GRK2 | LMNG | 4.0 | Y | N/A | N/A |
| | | WT | Arr2_3A | GRK2 | POPC/POPG ND | 3.0 | Y | N/A | N/A |
| | | +12G | Arr2_3A | GRK5 | LMNG | 3.6 | Y | N/A | N/A |

Structures highlighted in blue included the receptor micelle, whereas those in yellow did not, generally yielding higher resolution maps. Not all reconstructions were fit with an atomic model.

**Table S2. List of PDB entries used for PCA analysis and their PC1 and PC2 values.**

**Movies S1 & S2**. **Motions described by the PC1 and PC2 axes from PCA analysis, respectively.** The portion of arrestin structure used for PCA is shown as tube with its N- and C-lobes colored green and blue, respectively. Dashed lines indicate loops not used for PCA because of structural gaps among the compared structures. The range of motion is determined by 1.5-fold standard deviation of conformations along the PC in both directions from the mean conformation (PC values of 0). PC1 motion corresponds to a ~30° twist of the C-lobe relative to the N-lobe from lower to higher PC1 values. PC2 motion corresponds a ~5° “wag” of the C-lobe relative to the N-lobe.